Is the Earth Lazy? A review of work minimization in fault evolution

Michele L. Cooke* and Elizabeth H. Madden

Department of Geosciences
University of Massachusetts, Amherst
Amherst, MA 01003-9297 USA

Corresponding author: Michele Cooke
611 North Pleasant St., Amherst, MA 01003 USA
cooke@geo.umass.edu
+1 413 577-3142,

Keywords: work minimization; fault propagation; energy budget; numerical model

Abstract

The principle of work minimization has been used in various forms to account for the development of active fault systems within a wide range of tectonic settings. We review the successes, challenges and implications learned from previous applications of work minimization. Examination of the energy budget provides insight into the competing influences of different processes within fault systems at a variety of scales. We present each work budget component with considerations for numerical implementation. Additionally, we demonstrate numerical implementation by solving for the energy budgets and finding the most efficient propagation paths of a joint and several faults. Consideration of the energy budget captures growth patterns that are consistent with both laboratory observations and theoretical predictions using the energy release rate, G. Unlike using G, work minimization is not limited to collinear growth. In comparison with predictions using Coulomb failure planes, work minimization eliminates uncertainty in predicting fault propagation by (1) evaluating the trade-off between tensile and shear failure ahead of the fault and (2) avoiding the ambiguity introduced by the two potential Coulomb failure planes. Application of work minimization to faulting demonstrates the effectiveness of this approach in predicting both the orientation and timing of fault propagation.

1. Introduction

Crustal deformation results from complex plate motions acting on a variety of time scales, from the seconds required for earthquake ruptures to the millions of years required for mountain building. Brittle failure plays a large role in this deformation, as faults slip and grow to accommodate tectonic loading and dykes propagate due to internal magma pressure, for example. Predicting the growth of brittle structures is critical to unraveling many geophysical processes and is particularly important for understanding fault evolution.

Inglis (1913) provided fundamental insights into the role of concentrated stresses around flaws, and their role in flaw growth and the subsequent failure of the material. Using these insights, the growth of fractures can be predicted if the stress concentration factor at the fracture tip meets the strength of the material. This concept is fundamental to theories of linear elastic fracture mechanics and has been successful in predicting conditions for and paths of opening mode propagation that is characteristic of joints, veins and dikes in rock materials (e.g. Pollard and Aydin, 1988). Analysis of the propagation of faults using this approach has been more problematic. The challenges arise from the distributed nature of damage preceding fault growth and the subsequent linkage of cracks to form fault surfaces. The deformational processes around a fault tip do not match the in-line growth pattern required for using stress concentration factors to predict the potential for fault growth. In addition, while seismologists have been successful in using a local energy balance at the fracture tip to model earthquake dynamics, strength heterogeneities in the Earth make application of this approach over large areas and long time-scales particularly difficult.

In contrast, work minimization provides a global approach to predicting failure by postulating that the crust deforms in order to minimize the external tectonic work acting on it. This deformation includes the propagation of faults and work minimization suggests that fault propagation will occur in the direction that minimizes external energy. As a consequence, a fault system may evolve over geologic time to efficiently accommodate forcing from plate motions. A work minimization approach does not ignore fracture mechanics, but rather drives mechanics based on a global energy budget, rather than solely on a criterion local to the fault or fracture tip. Furthermore, fault growth along a mechanically efficient path can still require that local conditions for failure are met at a fault tip, though the timing and orientation of growth are based on the global energy budget.

While the principle of work minimization has been applied in various forms in the past, now is an ideal time to apply it to research on crustal deformation in general and fault behavior in particular. Current computing capabilities allow fault mechanics to be considered and the full energy budget of deformation to be determined. This eliminates resurgent concerns regarding minimization approaches, such as that strain minimization fails to capture the “complete energetics of the system” (Bird and Yuen, 1979). Computational advances also allow for better constraints on and quantification of individual work budget components, including the energy required in work against friction, energy required for propagation, energy converted into seismic waves, work against gravity, and the internal strain energy of the deforming system.

In this review paper, we present the individual components of the energy budget along with guides for numerical implementation of the calculations. Different approaches that previous investigators have taken to predict fault evolution using the principle of work minimization are outlined, as well as the historical debates about the appropriateness of work minimization in the study of fault network evolution. To demonstrate the benefits of analyzing the complete work budget, we apply work minimization to the growth of a joint and a fault, and contrast their energy budgets. The paper concludes with discussion of the insights provided by using a work minimization approach to investigate tectonic deformation in general and fault system evolution in particular, as well as on-going considerations for doing so and current challenges.

2. Energy budget for fault evolution

Prior to reviewing the contributions of previous investigations of fault evolution using work minimization, we outline the individual components of the energy budget. Over the years, various workers have used slightly different definitions of these energy terms and utilized different subsets of the complete energy budget. Here we present a set of consistent formulations for a complete energy budget associated with fault growth. This budget includes internal work of deformation around faults, W_{int}, work against gravity, W_{grav}, work against friction along faults, W_{fric}, energy to create fault surfaces, W_{prop}, and energy of ground shaking, W_{seis}. The sum of these terms equals the total work of the system, which is the external work, W_{ext}, along the boundaries of the fault system (Fig. 1):

$$W_{ext} = W_{int} + W_{grav} + W_{fric} + W_{prop} + W_{seis} \qquad \text{Eq. 1}$$

The internal work and work against gravity often are considered together as mechanical work. Within fault systems, gravitational force plays a different role within contractional and extensional systems (Dempsey et al., 2012), so separating these two work components provides relevant insights. All work terms except for the energy consumed by creating fault surfaces (W_{prop}) can be derived from the product of a force and a displacement within the fault system. In addition to describing the theoretical underpinning of each component of the work budget, we note special considerations for the numerical calculation of each component.

2.1 Internal work of deformation

Internal work is the work of deformation within the fault system. W_{int} can be measured as strain energy density, which is the product of stress and strain (e.g. Timoshenko and Goodier, 1951; Jaeger et al., 2007). The integral of the strain energy density within the fault system provides the internal work of the system:

$$W_{\text{int}} = \oiiint \frac{1}{2}\sigma_{ij}\varepsilon_{ij}dV \qquad \text{Eq. 2}$$

For a two-dimensional system in x-z space, Eq. 2 simplifies to:

$$W_{\text{int}} = \frac{1}{2}\iint \sigma_{xx}\varepsilon_{xx} + \sigma_{zz}\varepsilon_{zz} + 2\sigma_{xz}\varepsilon_{xz}dxdz \qquad \text{Eq.3}$$

Although the internal strain energy represents elastic recoverable strain, the internal work term also incorporates energy available for consumption by inelastic processes. For example, pervasive deformation mechanisms, such as calcite twinning, may reduce stresses within deformed host rock between faults and subsequently consume internal work. The role of distributed permanent deformation on the work budget has not yet been investigated. The strain energy density around faults is often greatest near fault tips and irregularities. Consequently, the internal work is a powerful control on fault propagation and many studies have predicted fault growth using minimization of internal work (Melosh and Williams, 1989; Du and Aydin, 1992; Du and Aydin, 1996; Okubo and Schulz, 2005). W_{int} is reversible, meaning that it can either increase or decrease during fault system evolution.

In the numerical implementation of W_{int}, the volume integral is calculated via sampling points throughout the model. In the absence of faults, integrating a volume of densely spaced sample points can provide accurate solutions for W_{int}; however, the discretization of the fault into elements introduces approximations to the stress field. Near fault tips, where stresses vary a lot over short distances, these approximations can impede accurate sampling of W_{int}. Of all of the work components, calculation of W_{int} has the greatest errors. Additionally, we need to consider that the total W_{int} is sensitive to the size of the fault system analyzed. For two models with identical fault length, but different model dimensions, the larger model will have greater W_{int}. For this reason, the difference in W_{int} before and after fault growth can be more informative than its total value.

2.2 Work against gravity

Gravitational work considers the upward displacement, d_z, against gravitational force, g,

$$W_{grav} = \oiiint \rho g d_z(z) dV \qquad \text{Eq. 4}$$

where ρ is the density of the material. Like W_{int}, W_{grav} is reversible and can increase or decrease during fault system evolution. Contractional fault systems will have an overall upward displacement of points within the system that result in a positive W_{grav} while extensional systems will have negative W_{grav}. Dempsey et al. (2012) show that a decrease in W_{grav} can drive extensional faulting, even at the expense of an increase in W_{int}. This complicates the elastic rebound paradigm of faulting, which was developed for strike slip faults and assumes that slip events are associated with a decreased in stored elastic energy. For all fault systems, decreases in the sum of W_{grav} and W_{int}, which is termed the mechanical work, provide energy for fault slip, propagation and ground shaking.

The numerical calculation of W_{grav} requires sampling the displacement field throughout the model. Unlike W_{int}, the displacements are not singular near the fault so calculations of W_{grav} are not as sensitive to numerical discretization of the fault as calculations of W_{int}. Both mechanical work terms are sensitive to the size of the model domain.

2.3 Work against frictional resistance

The frictional work is the energy required to slide fault surfaces past each other. W_{fric} is irreversible, because the heat created during frictional slip exits the system. The onset of sliding involves processes related to the work required to generate new fault surfaces and W_{fric} (Fig. 2A). The component attributed to work against frictional resistance is calculated from the strength of the fault at stable sliding and the total slip, s. For a single fault segment using a tension positive, compression negative sign convention, this component is calculated as:

$$W_{fric} = (c - \sigma_n \mu_d)sA = |\tau|sA \qquad \text{Eq. 5}$$

where c is cohesion, σ_n is normal stress, μ_d is the dynamic friction coefficient during sliding, τ is the shear strength during sliding, and A is the slipped area of the fault. When positive, σ_n is tensile along the fault and allows opening, so W_{fric} is zero. The complete frictional work for one increment of loading is integrated over the surface area, A, of the fault so that:

$$W_{fric} = \oiint [c - \sigma_n \mu_d] dA = \oiint \tau dA \qquad \text{Eq. 6}$$

Frictional work can be calculated as fault strength evolves over a loading increment (e.g. Savage and Cooke, 2010); however, most quasi-static studies use the stress state at the end of the model convergence to calculate W_{fric} (e.g. Hardy et al., 1998; Burbridge and Braun, 2002; Cooke and Murphy, 2004; Del Castello and Cooke, 2008). Because frictional work is inelastic, numerical implementations often load the faults system with multiple monotonic steps so that W_{fric} is calculated for each loading step and integrated over the applied loading (e.g. Cooke and Murphy, 2004; Del Castello and Cooke, 2008)(Fig. 2B).

Observations generally support the inference that mature faults have lower sliding friction than immature faults (e.g. Marone, 1998). Nevertheless, the formulation of W_{fric} is the same for the development of new fault surfaces and slip along mature fault surfaces. In addition, a new fault surface with high strength and low slip may produce identical frictional heating to a mature fault surface with low strength and high slip.

Until recently, we have not been able to measure the frictional heat produced by fault slip events. On-going projects that drill and sample active fault zones (e.g. Townend et al., 2009) and particularly efforts to drill soon after earthquake events (e.g. Fulton et al., 2013) are providing constraints on frictional heating so that we can validate the theoretical formulations. Studies of heating along exhumed faults are further constraining values of W_{fric} (Savage et al., 2014).

2.4 Seismic radiated energy

The strength of a fault evolves during slip, from the initial strength (τ_0) to the weakened sliding strength (τ) (Fig. 2A). This change in shear stress with slip produces energy that is available for both fault propagation, W_{prop}, and ground shaking, W_{seis}, which are irreversible and lost to the fault system. The portion of work allocated to each process depends on the amount of fault slip relative to the slip required to bring the fault to its sliding strength, referred to as the slip weakening distance, L (Fig. 2). All energy associated with the shear stress drop ($\Delta\tau = \tau_0 - \tau$) when s exceeds L is available for ground shaking. In other words, the energy required to generate the new fault surface is expended while $s < L$, whereas work associated with $s > L$ is available for ground shaking. If $L = 0$, W_{seis} for one increment of loading is:

$$W_{seis} = \oiint \int \Delta\tau \, ds \, dA \qquad \text{Eq. 7}$$

Numerical models typically do not consider the evolution of shear stress with slip and only calculate the change in shear stress, $\Delta\tau$, from comparing model results before and after fault growth. In this case, the work need not be integrated over slip and Eq. 7 simplifies to:

$$W_{seis} = \oiint \frac{1}{2} \Delta\tau \, s \, dA \qquad \text{Eq.8}$$

In the event of multiple loading increments, W_{seis} is calculated from the change in shear stress and the change in slip from one loading step to the next (Fig. 2B). The calculation of the W_{seis} is not largely affected by discretization.

The formulation of W_{seis} is the same for both established and new fault surfaces, but the values of τ and τ_0 may differ. For example, intact rock often requires greater shear stress to reach failure than an established fault surface. While quasi-static models cannot be used to calculate shaking directly, they can be used to examine $\Delta\tau$ and estimate the energy available for shaking.

2.5 Energy of fault propagation/growth

The energy of fault propagation, W_{prop}, is the energy required to create discontinuities within a material. This energy is irreversible within most natural conditions. Although Obriemoff (1930) was able to reverse the growth of a crack in mica by growing the crack within a vacuum, under atmospheric conditions, available cations bonded to new crack surfaces and impeded healing.

Griffith (1921) demonstrated that the energy release rate, G, required to grow a crack can be calculated directly from the stress intensity factors on the crack, K_i, where i refers to growth by modes I, II or III:

$$G = \frac{1-\upsilon^2}{E}\left[K_I^2 + K_{II}^2 + \frac{K_{III}^2}{(1-\nu)}\right] \qquad \text{Eq. 9}$$

Here, ν is Poisson's ratio and E is Young's Modulus. However, this formulation presumes co-linear crack propagation of a single discontinuity, so Eq. (8) works well for opening-mode propagation of joints and veins in rock, and is applicable for controlled experiments that result in co-linear growth. However, this formulation does not apply universally to faults, which often propagate out of plane. Consequently, predicting fault growth using G is problematic.

Taking an observational approach, some workers have estimated W_{prop} from measurements of damage around faults. Using the measured energy release rate of opening mode cracks ($G \cong 1$ J/m^2), the total energy consumed in fault growth can be estimated by summing the damage area around faults (e.g. Wong, 1982, 1986; Cox & Scholz, 1988). For cases of new faulting within intact rock, these values are 10^5-10^6 J/m^2 (Wilson et al., 2005; Pittarello et al., 2008). In contrast, values from laboratory samples range only up to 10^4 J/m^2 (Wong, 1982, 1986; Cox & Scholz, 1988; Lockner et al., 1992). These different ranges from laboratory and field measurements highlight the need to develop a better understanding of W_{prop}. In section 4, we present numerical models that simulate laboratory experiments of faults loaded at values critical for growth. In addition to demonstrating the work budget of fault growth, these experiments allow for calculation of W_{prop}. For co-linear propagation, this value can be validated against calculations of G.

A formula for W_{prop} that does not require co-linear growth is related to that for W_{seis}. As mentioned in the previous section, the portion of work allocated to each of these processes depends on the amount of fault slip, s, relative to the slip weakening distance, L (Fig. 2A). The energy required to generate the new fault surface is expended while $s < L$, whereas work associated with $s > L$ is available for ground shaking. For loading steps where the total slip remains less than L, this is:

$$W_{prop} = \oiint \frac{1}{2}\Delta\tau\Delta s dA \qquad \text{Eq. 10}$$

where Δs is the change in slip associated with that loading step and W_{seis} equals zero. For loading steps that produce slip that spans the slip weakening distance, such as step 3 on Fig. 2B, this is:

$$W_{prop} = \oiint \frac{1}{2} \Delta\tau s_L dA \quad \text{Eq. 11a}$$

$$W_{seis} = \oiint \frac{1}{2} \Delta\tau(\Delta s - s_L) dA \quad \text{Eq. 11b}$$

Here, s_L represents slip during this loading step when s < L. The total W_{prop} and W_{seis} for the system are summed at each loading step.

2.6 External work

The external work reflects the overall mechanical efficiency of the fault system, such that an efficient system will require less W_{ext} to accommodate the same tectonic displacement than an inefficient system. W_{ext} is the product of the shear and normal tractions, τ and σ_n, and shear and normal displacements, u_s and u_n, along the model boundaries, B (Fig. 1):

$$W_{ext} = \oiint \left(\tau u_s + \sigma_n u_n\right) dB \quad \text{Eq. 12}$$

If multiple loading steps are applied, the calculation of W_{ext} should be integrated over the loading steps. The value of W_{ext} also equals the sum of the energy budget components in Eq. (1). This relationship provides an independent check on the calculations of individual energy terms within the budget. Considerations of fault system evolution benefit from attention to changes in external work, ΔW_{ext}, between stages of fault growth. To meet requirements of energy conservation, we can consider that ΔW_{ext} equals the sum of the associated changes in all work budget components.

This energy budget differs from the energy considerations single earthquakes, where it is assumed that no change in remote loading or strain occurs during the short time-span of fault slip (e.g. Scholz, 2002). Under this assumption, which follows that presented by Griffith (1921), the change in mechanical work, $\Delta(W_{int} + W_{grav})$, equals the sum of the changes in W_{fric}, W_{prop} and W_{seis}. During an earthquake, the decrease in mechanical work provides the energy that is consumed in frictional heating, generation of damage, and ground shaking. The assumption that $\Delta W_{ext} = 0$ is not appropriate for studies of fault evolution, however, which consider fault development over multiple earthquake cycles due to tectonic loading. Consequently, we consider ΔW_{ext} as the fault system evolves, following the work of Del Castello and Cooke (2007), which shows that a fault system prefers to propagate in the direction that maximizes ΔW_{ext}.

The approach of analyzing the increasing efficiency of evolving fault systems in numerical models depends on the method of applied deformation, i.e. applied tractions or displacements. For fault systems that are loaded with displacement along the model boundaries, fault growth will increase the compliance of the system, so that the corresponding tractions along the model boundaries decrease. In this case, W_{ext} will decrease with the growth of more efficient faults within the system. In contrast, if the system is loaded with tractions along the model boundaries, then the increase in compliance due to fault growth will increase the displacement of the model boundaries. In this case, W_{ext} will increase with the growth of more efficient faults within the system. Either displacement or traction loading is suitable for a work budget analysis, but we advise against using mixed non-zero boundary conditions. In the cases of both displacement only and traction only loading, the most efficient fault growth path is that which maximizes the change in external work, ΔW_{ext}, from before to after fault growth. We demonstrate both types of loading in section 4, but continue to refer to growth that optimizes energy efficiency as "work minimization".

3. Work minimization in structural geology

For over a century, engineers have used energetic principles to understand material deformation and failure. Griffith (1921, 1924) used the energy budget associated with opening mode fracture growth to determine the equations governing fracture propagation, which launched the field of fracture mechanics. In an interesting revisitation of this classic approach, Engelder and Fisher (1996) execute Griffith's conceptual model within the laboratory and discuss implications for the loading of joints in the crust. Here, we review past applications of energy minimization to assess fault growth in detail. These studies present many interesting insights, as well as challenges that remain to be resolved.

Though we do not review them in detail, work minimization approaches have been used in other geoscience disciplines as well. For example, within metamorphic petrology, the numerical code ELLE predicts microstructure development based on work minimization of forces and chemical reactions within the system (e.g. Jessell et al, 2001). Modern fluvial geomorphology is founded on the work of Langbein and Leopold (1964), which analyzes the energy budget of evolving river channels. Another formulation of work minimization is maximum entropy. Rather than assessing the energy available within the system, the maximum entropy approach assesses the irreversible energy that is no longer available to the system. An example of this application is atmospheric circulation models that utilize maximum entropy to predict flow (e.g. Kleidon et al., 2003).

3.1 Minimum viscous dissipation

For several decades, the minimization of work has been utilized to predict the development of fault systems. The earliest approaches minimized the viscous dissipation within ocean ridge and transform fault systems. In this application, analytical solutions characterizing the system were solved to find the fault network that uses the least force to accommodate the prescribed plate boundary displacements via viscous flow within the fault zones. Lachenbruch and Thompson (1972) showed that minimum viscous dissipation predicts the orthogonal orientation of ridges and transform faults. This study was followed by several others that augmented this analysis to successfully account for various observations of ocean ridge geometry (Fig. 3) (e.g. Froidevaux, 1973; Stein, 1978; Kleinrock and Morgan, 1988). In 1979, Bird and Yuen published a critique of the approximations used in the analytical implementation of the minimum viscous dissipation approach. They pointed out that the approximations are avoided with numerical implementations that directly solve the governing equations and consider more complex rheology and coupled processes within the crust (e.g. Regenauer-Lieb et al., 2006; Holtzman et al., 2005). This critique was followed by a comment in support of the original methodology by Sleep et al. (1979).

A similar approach to minimizing viscous shear is minimizing on-fault shear stress, which has been used to predict the orientation of frictionally sliding faults. Reches (1983) implemented a minimum dissipation approach for frictionally sliding faults, which showed that sets of orthorhombic faults require the least shear stresses to accommodate three-dimensional states of strain. In this same study, Reches (1983) demonstrated that the fault networks that minimize shear stress also minimize the internal work in the rock between the sliding surfaces.

3.2. Minimization of internal work

More efficient fault systems allow for more fault slip, so that the surrounding rock is relatively less strained and subject to less stress. Consequently, the minimization of internal work, which integrates the product of the stress and strain fields Eq. (2), can achieve similar predictions of fault geometry as methods that minimize the forces required to accommodate prescribed deformation. Melosh and Williams (1989) demonstrated that antithetic pairs of normal faults result in lower internal work than synthetic pairs of normal faults. The greater efficiency of antithetic normal faults may account for the frequent occurrence of antithetic normal faults within grabens (Melosh and Williams, 1989). Hexagonal cracks within uniformly expanding materials, such as mud cracks, are another common observation that has been explained by the minimization of strain energy per unit of new crack area (Lachenbruch, 1962).

Within elastic systems, the spatial variations of internal work throughout a fault system can be mapped with the Strain Energy Density, SED, so that SED is the internal work at a point within the system. The distribution of SED has been used to assess the growth and propagation faults. This approach utilizes the premise that faults develop in regions of high stress and strain, so that the growth of faults should minimize the total SED, i.e. the internal work (e.g. Du and Aydin, 1993; Du and Aydin, 1996; Okubo and Schulz, 2005; Olson and Cooke, 2005). Following this approach, Olson and Cooke (2005) used three-dimensional models to compare fault orientations predicted by the locations of high SED with those predicted by Coulomb failure theory, and showed that locales of high SED better predict the interpreted evolution of imbricate thrust faults within the Los Angeles basin (Fig. 4). Griffith and Cooke (2004) used SED patterns around alternative three-dimensional configurations for the intersection of the Whittier and Puente Hills faults to show that the configuration that minimizes internal work also reproduces the observed slip rate.

Further insights can be gained by decomposing SED into its two deformational components, the dilatational and distortional strain energy densities (e.g. Jaeger et al., 2007). Because faults accommodate distortion, the pattern of faulting may be predicted by the maximization of distortional SED (e.g. Du and Aydin, 1992; Du and Aydin, 1996; Okubo and Schulz, 2005). Limiting analysis to the distortional SED is akin to using a maximum shear stress or second invariant of shear stress failure criterion, such as von Mise's criterion. While this approach does not consider the role of the normal stress, as Coulomb failure does, the predicted fault propagation patterns resemble general observations of fault step-overs (Du and Aydin, 1993) and the propagation path of deformation bands (Okubo and Schulz, 2005), as well as the development of the Eastern California Shear Zone north of a bend in the San Andreas fault in California, USA (Du and Aydin, 1996),. Furthermore, Okubo and Schulz (2005) used dilatational SED to predict fault initiation locations, which may be related to dilatational failure, in contrast to distortion dependent propagation processes. These studies demonstrate that faults grow into regions of high internal work, which consequently can reduce the W_{int} of the system.

Another application is in crustal models, where minimum internal work is used to interpolate deformation in regions where geologic data are scarce (e.g. Saucier and Humphries, 1993; Peltzer and Saucier; 1996). These models use geodetic velocities and geologic slip rates as input where they are available. Minimizing internal work provides a way to resolve slip along portions of the faults, while satisfying data constraints. The widespread use of this approach supports the premise that faults develop to minimize internal work.

A corollary to the minimization of internal work is the maximization of slip. The theory here is that the fault system with the least internal work will display the largest amount of fault slip. DeBremaecker and Ferris (2004) show that maximum slip predicts the orientation of wing-crack development at fault tips. Using analog experiments of restraining bends, Cooke et al. (2013) showed that the percentage of slip accommodated by fault systems increases with the propagation of new faults as the system becomes more efficient. This analog modeling study further supports the premise that faults evolve to greater efficiency by maximizing fault slip and minimizing internal work.

3.3 Minimization of strain

The calculation of either internal work or viscous dissipation requires solving for both the displacement (or velocity) and the stress (or stress rate) fields. An analytically more simple and computationally faster approach is to minimize only the strains or displacements. By assuming that locations of high stress are also locations of high strain, minimizing strain should have the same effect as minimizing internal work. The computational benefit is that the kinematic solutions can be used to find the strain field, without having to solve for stress. This approach has been used to assess the ratios of pure shear to simple shear during non-steady state deformation (Fossen and Tikoff, 1997). Following publication of that paper, Jiang (1998) criticized the minimum strain path approach, because it did not consider the full energetics of the system. In their reply, Fossen and Tikoff (1998) note that, due to the complexities of the system, it is not known if minimizing work gives a different result from the kinematic solutions found by minimizing strain. In many ways, this discussion and reply echo the discussion two decades prior between Bird and Yuen (1979) and Sleep et al. (1979).

Minimization of strain also is used in several applications to determine fault slip, when the system is under-constrained. Strain minimization can be used in a similar way to the minimization of internal work, to resolve unconstrained fault slip rates within crustal deformation models (e.g. Flech et al., 2001). Similarly, several three-dimensional structural restoration algorithms minimize strain to determine slip along faults within a system (e.g. Plesch et al., 2007; Shackleton et al., 2009).

3.4 Limit analysis

Limit analysis provides an alternative approach for finding the most efficient failure surface using analytical solutions. Like other methods, it draws from engineering mechanics and has a long history of success. For example, Bishop (1955) developed a standard method to investigate slope stability by delineating the most likely landslide surface as that which fails at the least applied stress. Similar methodology has been used to find the fault surface within an accretionary wedge that fails under the lowest force (e.g. Maillot and Leroy, 2003; Maillot and Leroy, 2006; Cubas et al., 2008; Souloumiac et al., 2009; Souloumiac et al., 2010; Mary et al., 2013). The limit analysis requires analysis of many potential surfaces to find the one that requires the minimum force to deform. This surface is at its failure limit, so it requires the 'least upper bound of applied force', a phrase often used in this literature. Lesser force can be applied, but the upper bound of force is that required for failure of the system, i.e. the development of faults. One of the great benefits of the limit analysis approach is that it is analytical, so that the search for the preferred surface completes within seconds. Consequently, limit analysis can be used to assess sequential failure of multiple surfaces and shows many of the same features as accretionary wedges (Fig. 5) (e.g. Cubas et al., 2008, Mary et al., 2013).

3.5. Minimization of total and external work

Many workers have recognized that internal work does not capture the complete system and so have sought to find the fault geometry that minimizes the system's total work. This total work represents different combinations of work budget components in different applications, including: 1) work against gravity, which is sometimes integrated with internal work, 2) work against friction, 3) energy required to propagate faults, and 4) seismic radiated energy (Fig. 1) (e.g. Cooke and Murphy, 2004). Jones and Wesnousky (1992) considered internal work and work against friction to demonstrate that under transpressional loading, slip partitioning between two parallel fault planes, one with dip slip and another with strike slip, minimizes the total work of the deforming system. Cooke and Kameda (2002) showed that, for a variety of proposed cross-sections of the Los Angeles basin, the system that requires the least total work to accommodate tectonic loading is that which best matches the available fault slip rates. In a study of the Lake Meade Fault zone, Marshall et al. (2010) assessed the relative efficiency of different fault interpretations. The configuration that minimizes work is consistent with independent observations and provides inside into interaction among faults. These studies lend support to the postulation that fault systems evolve to minimize total work.

By far, the bulk of investigations of fault evolution using work minimization with a full work budget analysis examine accretionary wedge systems. Both analog models and crustal wedges provide excellent laboratories for studying fault growth, because the material is relatively undeformed prior to incorporation into the wedge, while within many other deformational regimes, the rock mass may have inherited fault structures that complicate a minimum work analysis. Dahlen et al. (1984) is a watershed study that introduced the concept of critically tapered wedges. A few years later, Mitra and Boyer (1986) framed the development of duplexes, which can be viewed as the cellular unit of an accretionary wedge, in terms of the system's work budget. Dahlen et al. (1989), followed up with a work budget for the entire accretionary wedge that has been augmented by many workers (e.g. Gutcher et al., 1998; Hardy et al., 1998; Burbridge and Braun, 2002).

Several studies assess fault propagation within accretionary systems through minimization of the energy required to overcome friction and gravity (Gutscher et al., 1998; Hardy et al., 1998; Burbridge and Braun, 2002). Gutscher et al. (1998) showed analytically that minimization of frictional and gravitational work accurately predicts the length of a new accretionary forethrust. Burbidge and Braun (2002) extended this analysis to determine the friction required for frontal and back accretion, while Hardy et al. (1998) used a combined Eulerian-Lagrangian scheme within numerical models to minimize frictional and gravitational work to predict the progressive sequence of accretion. Masek and Duncan (1998) expanded these analyses by including internal work, showing that this component has a large influence on fault geometry. As with previous applications of work minimization, Masek and Duncan (1998) evoked a discussion and reply (DeBremaecker, 1999; Masek and Duncan, 1999). However, this discussion focuses on the effect of numerical discretization on the work budget, rather than on the premise of a fault growing to minimize work.

In a recent study of accretion, Del Castello and Cooke (2007) used a numerical implementation of work minimization to simulate analog experiments of accretion and present the evolving work budget during the process of new forethrust development (Fig. 6). In these finite models, the external work acting on the system represents the system's total work, and equals the sum of the five work budget components. A new forethrust reduces the external work required to deform the system due to a reduction in frictional work, even though the new fault increases the system's internal work (Fig. 6B). Additionally, the investigation of potential position and vergence of thrusts shows that the thrust in the numerical model that minimizes W_{ext} matches the forethrust that develops in the experimental sandbox. Del Castello and Cooke (2007) further found that propagation of the forethrust occurs when the decrease in external work due to adding the fault (ΔW_{ext}) exceeds the work required to create the new fault surface (W_{prop} + W_{seis}; Fig. 6C). This outcome highlights the critical role of the work of fault propagation, a work term not previously considered. This study suggests that consideration of external work and the work of fault propagation together allow for prediction of not only the path of fault propagation, but also the timing of fault propagation.

4. Work minimization predictions of fault propagation

To demonstrate the power of using a work minimization approach to study fault growth, we present the propagation paths and work budgets for co-linear growth of a joint and faults both with and without slip weakening. Following investigations by Del Castello and Cooke (2007), the most efficient growth paths are found by maximizing ΔW_{ext}, the difference in W_{ext} before and after propagation. Potential growth elements, or *pupative elements*, are radial to the fault tip at a prescribed range of angles to the fault. The growth of the fault via each pupative element is assessed separately and comparison of the results reveals the most efficient radial propagation path. The stresses along some pupative elements will not meet the tensile or shear failure criterion, so the fault will not be able to grow in these directions and W_{ext} remains unaltered (i.e. $\Delta W_{ext} = 0$). Among the pupative elements that do fail, the element that maximizes ΔW_{ext} is added to the initial structure. Though only one growth iteration is presented here, this sequence can be repeated for subsequent pupative elements.

We simulate joint and fault propagation under the conditions of laboratory experiments on fault growth by Bobet and Einstein (1998). Both the joint and the fault are 12.7 mm long and are comprised of 100 boundary elements of 0.127 mm embedded within a slab of gypsum (Fig. 7A, 7B). The pupative elements have the same length as elements along the pre-existing fault. The orientations of pupative elements are considered at 5°

angle increments between 45˚ and 315˚ clockwise from the joint or fault tip (Fig. 7B inset). We use the material properties for gypsum from Bobet and Einstein (1998) with a water to gypsum ratio of 0.4, tensile strength of 3.2 MPa, an average Poisson's ratio of 0.15, and an average Young's modulus of 5.96 GPa.

We utilize the two-dimensional boundary element method (BEM) program Fric2D (Cooke and Pollard, 1997). Dislocation surfaces made up of a series of elements of equal length are free to open or slip, but not to interpenetrate, in response to the tractions or displacement applied on model boundaries and interactions with other elements. Fric2D solves the quasi-static equations of deformation on all elements. We take a compression negative, tension positive sign convention. Elements fail in tension when the normal stress, σ_n, exceeds the prescribed tensile strength, T:

$$T \geq \sigma_n. \qquad \text{Eq. 13}$$

Shear failure is governed by a frictional failure criterion, so that an element along an established fault slips when the shear stress, τ, exceeds the frictional strength, which is the sum of cohesion, c, and the product of the coefficient of static friction, μ_s, and σ_n:

$$|\tau| \geq c - \mu_s \sigma_n \qquad \text{Eq. 14}$$

Fric2D also captures slip-weakening behavior (Savage and Cooke, 2010). When slip on a fault element exceeds a prescribed weakening distance, L, the friction evolves linearly from its static value, μ_s, to a dynamic value, μ_d.

The criterion governing the shear failure of intact rock has the same form as Eq. (14), but c is replaced by the rock's inherent shear strength, S_o, and μ_s is replaced by the coefficient of internal friction, μ_o:

$$|\tau_o| \geq S_o - \mu_o \sigma_n \qquad \text{Eq. 15}$$

Following onset of failure in intact rock, laboratory tests have shown that fault strength decreases as a fault surface develops during slip (e.g. Handin and Hager, 1957; Hazzard and Young, 2000; Mitchell and Lockner, 2008). In Fric2D, when a pupative element fails, its strength decreases so that shear stress drops from τ_o to τ as its internal friction value, μ_o, drops to μ_d. The inelastic behavior of frictional slip is solved iteratively until the model converges (Cooke and Pollard, 1997).

4.1 Joint propagation

In the joint model, we apply horizontal and vertical displacement boundary conditions, respectively u_h and u_v, on the edges of the gypsum block (Fig. 7A). Keeping $u_h=0$, we adjust u_v to its critical value, when the stress intensity factor, K_I, at the joint tip equals gypsum's mode I fracture toughness, K_{Ic}, of 0.15 MPa√m. This value of K_{Ic} value is from the curve reported by Chen et al. (2006, Fig.2), extrapolated to the 0.4 water to gypsum ratio used by Bobet and Einstein (1998). The failure criterion is met at $u_v=2.71e^{-5}$ m, which produces ~ 3.1 MPa of axial tension on the model boundaries.

Assessment of pupative elements around the joint tip reveals that the most efficient orientation for growth, the orientation that minimizes ΔW_{ext}, is at 180° (Fig. 8a). This co-linear growth is commonly observed for joints under perpendicular extension (e.g. Pollard and Aydin, 1988). W_{ext} is 1.1135 J before growth and drops to 1.1131 J after growth, resulting in ΔW_{ext} per pupative element area of -3.63 J/m^2. Note that, though the model is two-dimensional plane strain, all elements have a width of w = 1 m out of the plane under consideration. The components of the joint's work budget are summarized in Table 1 and Fig. 9. For this growth scenario, W_{seis}, W_{fric} and W_{grav} are 0, and $\Delta W_{int} = \Delta W_{ext} = W_{prop}$. Using Eq. (10), we find that W_{prop} = 3.62 J/m^2, which balances with ΔW_{ext}, indicating that the change in external and internal work is a result of energy spent on propagating the joint.

Because the joint growth is co-linear, we can compare this estimate of W_{prop} to that estimated by the critical energy release rate, G_c. Using K_{Ic} = 0.15 MPa√m, we find from Eq. (9) that G_c = 3.71 J/m^2. Thus, $\Delta W_{ext} \cong W_{prop} \cong G_c$, demonstrating consistency between opening-mode joint growth by work minimization and the theory outlined by Griffith (1921) for co-linearly propagating cracks.

4.2 Fault Propagation (Fault 1)

For the more complex scenario of fault growth, we began with two widely spaced, 60° dipping faults in gypsum that demonstrate co-linear growth under biaxial loading (scenario 60°-2a-4a from Bobet and Einstein (1998)). While Bobet and Einstein (1998) suggest that faults with internal tips at least 3 half-lengths (19.05 mm) from one another behave as isolated faults, the numerical simulations show some interaction between the stress fields surrounding these faults, even at 28.40 mm of internal tip spacing. To remove the effects of any interaction, we include only one fault in these simulations of fault growth (Fig. 7B). While this geometry results in a slight overestimate of work budget components, it provides a more robust demonstration of isolated fault growth patterns under biaxial loading.

The numerical model for Fault 1 contains a pre-existing fault of 12.7 mm dipping 60°, with zero cohesion and equal static and sliding friction coefficients ($\mu_s = \mu_d = 0.3$) (Bobet, 2000). The coefficient of internal friction on potential growth elements, μ_o, also is 0.3. The inherent shear strength, S_o = 78.7 MPa, for the growth elements is found by solving Eq. (15) using the critical shear and normal stresses on the element oriented at 180° from the fault tip at the onset of fault propagation (Fig. 7B) (Bobet, 1997, Table 4.2; Bobet and Einstein, 1998). We apply traction boundary conditions on the horizontal and vertical edges of the gypsum block of σ_h = -2.5 MPa and σ_v = -29 MPa, respectively (Bobet and Einstein, 1998).

ΔW_{ext} is largest for the pupative growth element oriented at 180° from the fault tip (Fig. 8b), consistent with the experimental observations of co-linear growth. The complete work budget for Fault 1 is compared with that for the joint in Fig. 9 and Table 1. For growth of 1 element length of 0.127 mm, W_{ext} increases from 878.5522 J to 878.5947 J. In contrast to the joint model, which used displacement boundary conditions so that a decrease in W_{ext} indicates an increase in efficiency, in this model an increase in W_{ext} indicates an increase in efficiency (see discussion in Section 2.6). This results in a ΔW_{ext} per pupative element area of 333.83 J/m^2. For this scenario, W_{seis} and W_{grav} are zero and $\Delta W_{ext} = \Delta W_{int} + \Delta W_{fric} = W_{prop} + \Delta W_{fric}$. Using Eq. (6) and Eq. (10), we find that W_{fric} = 79.78 J/m^2 and W_{prop} = 260.77 J/m^2. The sum of W_{fric} and W_{prop} is 340.54 J/m^2, which balances with ΔW_{ext}, indicating that the change in external work results from energy spent on fault propagation and the increase in frictional sliding that fault growth allows.

As for the joint, this co-linear propagation allows for a comparison of the fault's W_{prop} with that estimated by the critical energy release rate, G_c. Using the fracture toughness reported by Fric2D at the fault tip at critical loading (K_{IIc} = -1.27 MPa$\sqrt{\text{m}}$), we find that the critical energy release rate is G_c = 263.1 J/m^2. Thus, G_c is consistent with the work required for fault growth calculated using a work budget approach.

This model demonstrates the robustness of using a work minimization approach to model fault growth. Because this approach considers the global ΔW_{ext} instead of the local K_{IIc}, it can be applied to more complex fault propagation situations and is not restricted to co-linear growth. The work minimization approach also provides an estimate of the energy required for breaking intact rock to form new fault surfaces. In this case, we find that W_{prop} for fault growth in gypsum is 260.77 J/m^2. This value is reasonable, at two orders of magnitude larger than W_{prop} for joint growth in gypsum and several orders of magnitude smaller than the work inferred to grow faults in rock (10^4-10^6 J/m^2) (Wong, 1982, 1986; Cox & Scholz, 1988; Lockner et al., 1992; Wilson et al., 2005; Pittarello et al., 2008).

4.3 Propagation of slip-weakening faults (Fault 2, Fault 3)

We consider slip-weakening along pupative growth elements in two additional scenarios, Fault 2 and Fault 3. We prescribe μ_o = 0.6 and μ_d = 0.3 along both faults, but vary the weakening distance, L, over which the drop in friction from μ_o to μ_d occurs. L = 4x10^{-6} m for Fault 2 and L = 1x10^{-6} m for Fault 3. The shear stress drop resulting from slip weakening has the potential to produce seismic radiated energy, W_{seis} in addition to W_{prop} (Fig. 2).

As shown in Table 1 and Fig. 9, varying L does not change the angle of the pupative element that maximizes efficiency, which remains at 180° for both Fault 2 and Fault 3, nor does it change ΔW_{int} or ΔW_{fric}. However, L does affect the partitioning of work between fault propagation, W_{prop}, and the production of seismic waves, W_{seis} (Fig. 2). Shorter L (Fault 3) means that less energy is required to break the intact rock ahead of the fault, leaving more energy for ground shaking.

4.4 Comparison of work minimization and the Coulomb criterion

Correspondence between the maximum mechanical efficiency prediction of a fault's propagation path with that observed in laboratory experiments supports the use of work minimization as a fault growth criterion. This implementation of the principle of work minimization using numerical models utilizes Coulomb theory as a failure criterion for both the potential growth elements extending from the fault tip and those along the pre-existing fault surface. However, this approach differs from Coulomb stress analyses that determine a fault's propagation path from planes of maximum Coulomb shear stress out ahead of a fault tip. We compare the two approaches here.

The Coulomb shear stress is found on a potential failure surface by rearranging Eq. (15) to isolate S_o, replacing it with the Coulomb stress, σ_c, and replacing the frictional shear strength, τ_o, with the shear stress resolved on the surface, τ:

$$\sigma_c = |\tau| + \mu_o \sigma_n \qquad \text{Eq. 16}$$

Positive σ_c along a surface indicates that it has the potential for failure, while negative σ_c indicates that failure is inhibited. σ_c is useful for finding the relative failure potentials of different fault surfaces.

The potential failure planes that maximize σ_c are at angles of $\pm\varphi$ to the maximum compressive stress, σ_3. φ depends upon the inherent friction coefficient, μ_o:

$$\pm\varphi = \tfrac{1}{2}\,\mathrm{atan}(1/\mu_o) \qquad \text{Eq. 17}$$

The ± indicates that Coulomb theory predicts two potential planes, on either side of σ_3, that carry the same shear stress magnitude and therefore the same failure potential. Selecting between these planes is not trivial.

For this analysis, we consider both Coulomb and tensile failure near the fault tip. Fig. 10A shows the orientations of planes carrying the maximum tension and Coulomb stress, . Figs. 10B and 10C display the contours of the maximum tensile stress and Coulomb stress, respectively, following fault slip and prior to fault propagation. In Fig. 10B, tensile stress is largest below and to the right of the fault tip, within the tensile quadrant of this left-lateral fault. Tension values exceed the tensile strength of 3.2 MPa in much of this region. Fig. 10C shows that the maximum Coulomb stress is located out ahead of the fault tip. The Coulomb stress fails to exceed the inherent strength of the gypsum (S_o = 78.7 MPa) in much of this region, except for directly in front of the fault. If we focus in the vicinity of growth, at half of 1 element length (0.0635 mm) from the fault tip (Fig. 10D), the Coulomb stress reaches 87.1 MPa and exceeds the shear strength of the rock. In addition, σ_1 = 72.3 MPa at this location, exceeding the tensile strength of the gypsum (T = 3.2 MPa). T is exceeded at the two locations to the right of the fault tip as well, where σ_1 = 82.2 MPa and 75.4 MPa.

Predicting the propagation path from these results is problematic. First, tensile stresses are large and exceed the tensile strength of the rock in multiple locations. This suggests that tensile failure in the form of a wing crack off the tip of the fault would occur prior to any failure in shear. Second, ignoring the potential for tensile failure, both Coulomb planes at the location where the shear strength is exceeded out ahead of the fault tip have equal potential for failure. The plane with left-lateral slip aligns with the pre-existing fault and may be the better candidate for fault growth in this scenario, but such a determination is difficult to automate, as it may not be possible in other scenarios. Furthermore, selecting incorrectly will greatly alter the prediction of any subsequent growth.

Using a work minimization approach has the advantage of evaluating both tensile and shear failure by another metric, in this case the energy efficiency of the system, and consequently avoids this fault plane ambiguity. The tensile failure of wing cracks is considered explicitly within the work minimization analysis, but under the loading used here, wing cracks are not as efficient as in-plane fault propagation. Considering the tensile failure and Coulomb failure independently at points ahead of the fault does not provide insights in the competition between these two mechanisms. In addition, within the work minimization approach, a pupative growth element is evaluated as a continuation of the pre-existing fault and experiences the slip and stress associated with that configuration. For many scenarios, this provides an advantage over evaluating slip at a point ahead of the fault tip. While the process zone around the fault tip no doubt includes microcracks that are not radial to the fault tip, consideration of tip-radial propagation conveniently considers the overall fault propagation path.

5. Implications

Examination of the complete energy budget provides insight into the competing influences of different processes within deforming fault systems. In an innovative study of multilayer folding, Ismat (2008) uses work minimization to explore the competition between different flexural mechanisms within the competent and incompetent layers of an evolving fold. Because gravity controls the growth of accretionary wedges, we might expect gravitational work to be the largest part of the accretionary experiment energy budget. DelCastello and Cooke (2007) showed that, within sandbox models of accretion, the greatest energy is consumed by the work of against friction. The frictional work arises from the weight of the overlying material, so gravity also plays a role in this scenario. The growth of new faults in front of the wedge serves to decrease frictional work, at the expense of an increase in internal work. The full work-budget analysis undertaken by DelCastello and Cooke (2007) revealed this complex trade-off between different components of the work budget. At a much larger scale, Meade (2013) showed that, within crustal scale models, internal work is the dominant energy sink. Thus, different systems require attention to different components of the work budget.

One challenge for any work budget investigation of fault systems is the appropriate bounds for the system. Consider a complex network of active faults, such as at the boundary of the Pacific and North American plates in southern California. Perhaps this system has evolved to minimize work at the plate boundary scale, but can we extract portions of this system (e.g. the Los Angeles basin) and reliably assume that this portion should also minimize work? It could be that local mechanical inefficiencies develop within a system that is efficient overall. If the system under consideration within the model is too constrained in scale, then we may not be allowing for local inefficiencies to arise. Another way to think of this is that we do not yet know if work minimization predictions of fault evolution are independent of scale.

Another challenge in work minimization analyses is that active fault systems do not always realize the most efficient configuration. We see this within sandbox models of accretion, where underthrusting persists until a new fault can grow, even though a new fault would be more efficient much earlier in the deformation (Fig. 6) (DelCastello and Cooke, 2007). However, growth of this new thrust fault is not possible until the system has enough energy to form the new fault surface. This energy requirement suggests that the degree of inefficiency that a fault system can tolerate depends on the strength of the crust, as well as on the details of the fault network geometry. It may be that inefficient fault configurations persist longer in regions of thick-skinned tectonics, where crustal strength is high, than in accretionary systems, where material is weaker.

We now have the tools and methods to make great advances in the study of fault system evolution via work minimization. In the application demonstrated here using numerical simulations of laboratory experiments, minimum external work determines the direction of the most efficient fault propagation path, whether the pupative element fails by in tension or shear. Elements that do not fail by one of these criteria do not alter W_{ext}, so the efficiency of the system is unchanged. Thus, by utilizing these failure criteria along pupative elements, the principle of work minimization is applied and theories governing fault mechanics are honored. This approach has the advantage of accommodating both in-line growth and growth at angles to pre-existing faults without invoking separate tensile and shear failure criteria that require parallel analyses. The work minimization approach also proves to be a viable alternative to using Coulomb theory, which empirically captures the physics of faulting, but is limited in its ability to predict propagation at fault tips. The main limitation is in generation of two equally viable potential failure planes. While one of the failure planes may match the observations of fault growth, Coulomb theory does not provide a means for objectively picking one plane over the other. While Coulomb theory is remarkably helpful for predicting failure of pre-existing structures, or comparing failure potential between multiple fault surfaces, ,it may not be so for predicting fault propagation and evolution.

We see two main applications of the principle of work minimization to analyses of geologic structure. The first is to use the full energy budget, or its individual components, to gain insight into processes of deformation. For example, recent work by Savage et al. (2014) constrained the energy required for fault frictional heating by estimating temperatures from biomarkers near an exhumed fault. Work against friction also was estimated recently by Fulton et al. (2013) from in-situ measurements of a fault that failed in the 2011 Tohoku earthquake. Similarly, the work budget within accretionary systems has shed light on the tradeoffs of underthrusting and accretionary phases in wedge development (e.g. Gutscher et al., 1998; Hardy et al., 1998; Burbridge and Braun, 2002; Del Castello and Cooke, 2007; Mary et al., 2013). Other studies that could benefit from similar analyses include the partitioning of off-fault deformation between different faults, the trade-off between various processes and uplift against gravity, and how different faulting scenarios affect estimates of the energy available for seismic shaking.

The second application of work minimization to structural geology is the prediction of fault propagation paths. This analysis has been done by comparing the total or external work of different interpretions of fault configurations along the southern San Andreas fault over the past 500,000 years (Cooke and Dair, 2011). Alternatively, work minimization can be used in conjunction with numerical modeling tools to predict propagation paths over multiple growth cycles, as presented here. The development of software to automate this process would provide powerful tools for predicting fault growth.

Acknowledgements

Jess McBeck provided invaluable software support for the project. The manuscript was greatly improved by reviews by Bill Dunne, Tom Blenkinsop and an anonymous reviewer. This work was supported by NSF EAR grant 1219919.

References

Bird, P., and D. A. Yuen, 1979. The use of minimum dissipation principle in tectonophysics, Earth and Planetary Sciences Letters, 45, 214–217.

Bishop, A. W., 1955. The use of the slip circle in the stability analysis of slopes, Géotechnique 5, doi:10.1680/geot.1955.5.1.7.

Bobet, A. and H. H. Einstein, 1998. Fracture coalescence in rock-like materials under uniaxial and biaxial compression, International Journal of Rock Mechanics and Mining Sciences, 35, 863-888.

Burbidge, D. R., and J. Braun, 2002. Numerical models of the evolution of accretionary wedges and fold-and-thrust belts using the distinct-element method, Geophysics Journal International, 148, 542– 561.

Cooke, M. L. and L. C. Dair, 2011. Simulating the recent evolution of the southern big bend of the San Andreas fault, Southern California, Journal of Geophysical Research, Solid Earth, 116, B04405, doi:10.1029/2010JB007835.

Cooke, M. L. and S. Murphy, 2004. Assessing the work budget and efficiency of fault systems using mechanical models, Journal of Geophysical Research, 109, doi:10.1029/2004JB002968.

Cooke, M. L. and D. D. Pollard, 1997. Bedding plane slip in initial stages of fault-related folding Journal of Structural Geology, 19, pp. 567-581.

Cooke, M. L. and A. Kameda 2002, Mechanical Fault Interaction within the Los Angeles Basin: A Two-Dimensional Analysis using Mechanical Efficiency, Journal of Geophysical Research, 107, doi:10.1029/2001JB000542

Cooke, M. L., M. T. Schottenfeld and S. W. Buchanan, 2013. Evolution of Fault Efficiency at Restraining Bends within Wet Kaolin, Journal of Structural Geology, doi:10.1016/j.jsg.2013.01.010.

Cox, S. J. D. and C. H. Scholz, 1988. On the formation and growth of faults: an experimental study, Journal of Structural Geology, 10, 413–430.

Cubas, N., Leroy, Y.M., Maillot, B., 2008. Prediction of thrusting sequences in accretionnary wedges. Journal of Geophysical Research 113, doi:10.1029/2008JB005717.

Dahlen, F. A., J. Suppe, and D. Davis, 1984. Mechanics of fold-and-thrust belts and accretionary wedges: Cohesive Coulomb theory, Journal of Geophysical Research, 89, 87–101.

Dahlen, F. A., 1988. Mechanical energy budget of a fold-and-thrust belt, Nature, 331, 335-337.

DeBremaecker, J.-C., 1999. Comment on “Minimum-work mountain building” by Jeffrey G. Masek and Christopher C. Duncan, Journal of Geophysical Research, 104, 20395.

DeBremaecker, J.-C. and M. C. Ferris, 2004. Numerical models of shear fracture propagation, Engineering Fracture Mechanics, 71, 2161-2178.

Del Castello, M. and M. L. Cooke, 2007. Underthrusting-accretion cycle: Work budget as revealed by the boundary element method, Journal of Geophysical Research, 112, doi:10.1029/2007JB004997.

Dempsey, D, S. Ellis, R. Archer and J Rowland, 2012. Energetics of normal faults earthquakes on dip slip faults, Geology, p79–282; doi:10.1130/G32643.1.

Du, Y., and Aydin, A., 1993, The maximum distortional strain energy density criterion for shear fracture propagation with applications to the growth paths of en echelon faults: Geophysical Research Letters, 20, p. 1091–1094.

Du, Y. and A. Aydin, 1996. Is the San Andreas big bend responsible for the Landers earthquake and eastern California shear zone, Geology, 24, 219–222.

Ellis, S., G. Schreurs, and M. Panien, 2004. Comparisons between analogue and numerical models of thrust wedge development, Journal of Structural Geology, 26, 1659–1675.

Engelder, T. and M. Fisher, 1996. Loading configurations and driving mechanisms for joints based on the Griffith energy-balance concept, Tectonophysics, 256, 253-277.

Fossen, H. and B. Tikoff, 1997. Forward modeling of non-steady-state deformations and the 'minimum strain path', Journal of Structural Geology, 19, 987-996.

Fossen, H. and B. Tikoff, 1998. Forward modeling of non-steady-state deformations and the `minimum strain path': Reply, Journal of Structural Geology, 20, 979-981.

Froidevaux, C., 1973. Energy dissipation and geometric structure at spreading plate boundaries, Earth and Planetary Science Letters, 20, 419-424.

Fulton, P. M.; Brodsky, E. E.; Kano, Y.; Mori, J.; Chester, F.; Ishikawa, T.; Harris, R. N.; Lin, W.; Eguchi, N.; Toczko, S., 2013. Low coseismic friction on the Tohoku-Oki fault determined from temperature measurements, Science, 342, 1214-1217.

Gutscher, M. A., N. Kukowski, J. Malavieille, and S. Lallemand (1998), Episodic imbricate thrusting and underthrusting: Analog experiments and mechanical analysis applied to the Alaskan Accretionary Wedge, Journal of Geophysical Research, 103, 10,161– 10,176.

Griffith, A.A., 1920. The phenomena of rupture and flow in solids. Philos. Trans. R. Soc. London, A, 221, 163-198.

Griffith, A.A., 1924. Theory of rupture. Proc. First International Congress Applied Mechanics, Delft, pp. 55-63.

Griffith, W. A. and M. L. Cooke, 2004. Mechanical validation of the three-dimensional intersection geometry between the Puente Hills blind-thrust system and the Whittier fault, Los Angeles, California, Bulletin of the Seismological Society of America, 94, 493-

505.

Handin, J. and R. V., Hager Jr, 1957. Experimental deformation of sedimentary rocks under confining pressure: tests at room temperature on dry samples. *AAPG Bulletin*, *41*, 1, 1-50.

Hardy, S., C. Duncan, J. Masek and D. Brown, 1998. Minimum work, fault activity and the growth of critical wedges in fold and thrust belts, Basin Research, 10, 365-373, doi: 10.1046/j.1365-2117.1998.00073.x

Hazzard, J. F. and R.P. Young, 2000. Simulating acoustic emissions in bonded-particle models of rock International Journal of Rock Mechanics and Mining Sciences 37, 867-872,

Holtzman, B., D. Kohlstedt and J.P. Morgan, 2005. Viscous energy dissipation and strain partitioning in partially molten rocks, Journal of Petrology, 46, 2569-2592, doi:10.1093/petrology/egi065.

Inglis, C. E., 1913. Stresses in a plate due to the presence of cracks and sharp corners, Fifty-fourth Session of the Institution of Naval Architects.

Ismat, Z., 2008. Energy budget during fold tightening of a multilayer fold, Journal of Structural Geology, 31, 972-988, 10.1016/j.jsg.2008.10.006

Jaeger, J. C., N. G. Cook, R. W. Zimmerman, 2007. Fundamentals of Rock Mechanics, 513 pp., Malden, MA.

Jessell, M., P. Bons, L. Evans, T. Barr and K. Stewe, 2001, Elle: the numerical simulation of metamorphic and deformation microstructures, Computers and Geosciences, 27, 17–30.

Jian, D., 1998. Forward modeling of non-steady-state deformations and the `minimum strain path': Discussion, Journal of Structural Geology, 20, 975-977.

Jones, C.H., and S.G. Wesnousky, 1992. Variations in strength and slip rate along the San Andreas Fault system, Science, 256, 83-86.

Kleinrock, M. C. and J. P. Morgan, 1988. Triple junction reorganization, Journal of Geophysical Research, 93, 2981–2996, DOI: 10.1029/JB093iB04p02981

Kleidon, A., K. Fraedrich, T. Kunz, and F. Lunkeit, 2003, The atmospheric circulation and states of maximum entropy production, Geophysical Research Letters, 30, 2223, doi:10.1029/2003GL018363, 2003

Lachenbruch, A. H., 1962, Mechanics of thermal contraction cracks and ice-wedge polygons in permafrost, Geological Society of Special Papers 1962, v. 70, p. 1-66, Americadoi: 10.1130/SPE70-p1GSA.

Lachenbruch, A. H. and G. A. Thompson, 1972. Oceanic ridges and transform faults: their intersection angles and resistance to plate motion, Earth and Planetary Sciences Letters, 15, 116–122.

Langbein, L. B. and W. B. Leopold, 1964. Quasi-equilibrium states in channel morphology, American Journal of Science, 262, 782-794, doi:10.2475/ajs.262.6.782.

Lin, W., Conin, M., Moore, J. C., Chester, F. M., Nakamura, Y., Mori, J. J., … Expedition 343 Scientists, 2013. Stress state in the largest displacement area of the 2011 Tohoku-Oki earthquake. Science, 339, 687-690, doi: 10.1126/science.1229379

Mary, B. C. L., B. Maillot and Y. M. Leroy, 2013. Deterministic Chaos in frictional wedges revealed by convergence analysis. International journal of numerical and analytical methods in geomechanics, DOI: 10.1002/nag.2177

Marone, C., 1998. Laboratory-derived friction laws and their application to seismic faulting: Annual Review of Earth and Planetary Sciences, 26, 643–696, doi: 10.1146/annurev.earth.26.1.643.

Marshall, S. T., S. A. Kattenhorn and M. L. Cooke, 2010. Secondary normal faulting in the Lake Mead fault system and implications for regional fault mechanics, *in* Umhoefer, P.J., Beard, L.S., and Lamb, M.A., eds., *Miocene Tectonics of the Lake Mead Region, Central Basin and Range*: Geological Society of America Special Paper 463, p. 289–310, doi: 10.1130/2010.2463(13).

Masek, J. G., and C. C. Duncan, 1998. Minimum-work mountain building, Journal of Geophysical Research, 103, 907– 917.

McKenzie, D. and J. Jackson, 1983, The relationships between strain rates, crustal thickening paleomagnetism, finite strain and fault movements within a deforming fault zone, Earth and Planetary Sciences Letters, 65, 182–202.

Meade, B, 2013. Revisiting the orogenic energy balance in the western Taiwan orogen with weak faults, Terra Nova, v. 25, 160-164, DOI: 10.1111/ter.12022

Melosh, H. J., and C. A. Williams Jr., 1989. Mechanics of graben formation in crustal rocks: A finite element analysis, Journal of Geophysical Research, 94, 13,961– 13,973.

Mitchell, T. M., and D. R. Faulkner, 2008. Experimental measurements of permeability evolution during triaxial compression of initially intact crystalline rocks and implications for fluid flow in fault zones, Journal of Geophysical Research, 113, doi:10.1029/2008JB005588.

Mitra, G., and S. E. Boyer (1986), Energy balance and deformation mechanisms of duplexes, Journal of Structural Geology, 8, 291– 304.

Obriemoff, J. W., 1930. The splitting strength of mica. Proceedings of the Royal Society of London, 127 A. 290-297.

Okubo, C. H., and R. A. Schultz, 2005. Evolution of damage zone geometry and intensity in porous sandstone: Insight gained from strain energy density, Journal of the Geological Society of London, 162, 939–949.

Olson, E. and M. L. Cooke, 2005. Application of Three Fault Growth Criteria to the Puente Hills Thrust System, Los Angeles, California, USA, Journal of Structural Geology, vol. 27, 1765-1777.

Peltzer, G and F. Saucier ,1996. Present-day kinematics of Asia derived from geologic fault rates, Journal of Geophysical Research, 101, 27943–27956, DOI: 10.1029/96JB02698

Pittarello, L., G. Di Toro, A. Bizzarri, G. Pennacchioni, J. Hadizadeh, M. Cocco, 2008. Energy partitioning during seismic slip in pseudotachylyte-bearing faults (Gole Larghe Fault, Adamello, Italy), Earth and Planetary Science Letters, 269,131–139, doi:10.1016/j.epsl.2008.01.052

Plesch, A., J.H. Shaw and D. Kronman, 2007. Mechanics of low-relief detachment folding in the Bajiaochang Field, Sichuan Basin, China, AAPG Bulletin, 91(11):1559-1575.

Pollard, D. and A. Aydin, 1998. Progress in understanding jointing over the past century, Geological Society of America Bulletin, v. 100, 1181-1204.

Reches, Z., 1983. Faulting of rocks in three-dimensional strain fields II. Theoretical analysis, Tectonophysics, 95, 133-156.

Regenauer-Lieb, K., R. F. Weinberg and G. Rosenbaum, 2006. The effect of energy feedbacks on continental strength, Nature, 442, doi:10.1038/nature04868

Savage, H. M. and M. L. Cooke, 2010. Unlocking the effects of friction on fault damage zones, Journal of Structural Geology, 1732-1741, doi:10.1016/j.jsg.2009.08.014

Savage, H. M., P. J. Polissar, R. Sheppard, C. D. Rowe and E. E. Brodsky, 2014. Biomarkers heat up during earthquakes: New evidence of seismic slip in the rock record, Geology, 2, 99-102.

Scholz . C H. 2002. The mechanics of earthquakes and faulting, second edition, Cambridge,University Press.

Shackleton, J.R., Cooke, M.L., Seed, G., and Gibbs, A., 2009, Three-Dimensional Modelling of Sant Corneli Anticline (Spain) Using a Hybrid-Geometric/Geomechanical Approach. 2009, AAPG Annual Convention and Exhibition, Denver, Colorado.

Sleep, N. H., S. Stein, R. J. Geller, and R. G. Gordon, 1979. Comment on ‘‘The use of the minimum-dissipation principle in tectonophysics’’ by P. Bird and D. A. Yuen, Earth and Planetary Sciences Letters, 45, 218– 220.

Stein, S., 1978. A model for the relation between spreading rate and oblique spreading, Earth and Planetary Sciences Letters, 39, 313-318.

Timoshenko, S. P. and J. N. Goodier, 1934. Theory of Elasticity, McGraw-Hill, New York.

Wilson, B., Dewers, T., Reches, Z., Brune, J., 2005. Particle size and energetics of gouge from earthquake rupture zones. Nature 434, 749–752.

Wong, T. F., 1982. Shear fracture energy of Westerly granite from postfailure behavior, J. Geophysical Research, 87, 990–1000.

Wong, T. F., 1986. On the normal stress dependence of the shear fracture energy, in

Earthquake Source Mechanics, Geophysics Monograph Series, 37, edited by S. Das, J. Boatwright, and C. H. Scholz, pp. 1 – 12, AGU, Washington, D. C.

Figures

Figure 1. Schematic of fault deformation shows the tectonic work (W_{ext}), internal work of deformation (W_{int}), work of uplift against gravity (W_{grav}), the work against frictional slip (W_{fric}), the energy required to grow a fault (W_{prop}) and the radiated seismic energy (W_{seis}). Taken from Cooke and Murphy, 2004.

Figure 2. Schematic of the partitioning of frictional heating, the energy required for fault growth and energy available for seismic shaking. Work is done when fault slips and the shear stress drops from the initial value, τ_o, to the value at stable sliding, τ. One can delineate the associated work terms in different ways. In most studies, W_{fric} is defined as the energy due to slip under sliding shear stress, consequently W_{fric} depends on absolute stress. The two energy terms that are consumed by fault growth (W_{seis} and W_{fric}) depend on the shear stress drop during the slip event. Prior to the slip reaching the slip weakening distance, L, work is primary consumed by the generation of new fault surface area (W_{prop}) and W_{fric}. Slip beyond the slip weakening distance produces W_{fric} and seismic radiated energy (W_{seis}). While the sketch in (A) shows this relationship for a single increment of loading the hypothetical sketch in (B) shows how W_{fric}, W_{prop} and W_{seis} are calculated over multiple loading increments, which are typically implemented within numerical models.

Figure 3. Minimum viscous dissipation demonstrates that of the possible ocean ridge (red) and transform (blue) intersections, several of which are show here, geometry (C) is the most efficient. Modified from Lachenbruch and Thompson, 1972.

Figure 4. A) Strain energy density (SED) and B) Coulomb stress for the interpreted Puente Hills fault system prior to the growth of the Coyote Hills fault (CH) in southern California. The region of high SED envelops the location of the Coyote Hills fault. If we use high SED and extreme values of Coulomb stress to predict the development of the next fault, the SED pattern gives a better correlation with the location of the observed fault. The Coulomb stress is less conclusive than the SED and suggests that the next faults may develop either northeast or southwest of the Whittier fault. Taken from Olson and Cooke, 2005.

Figure 5. (A) Limit analysis can be used to predict the sequence of thrusting. (B) The predicted evolution of the tectonic force shows drops in force with the growth of new

faults. Taken from Cubas et al. (2008).

Figure 6. DelCastello and Cooke (2007) explored the evolving work budget of forethrust growth within the analog experiments of Adam (2005). (A) The numerical models simulate lengthening of the thrust sheet prior to forethrust development. (B) With lengthening of the thrust sheet length, W_{fric} increases as the fault normal compression increases due to the thickening wedge. Consequently, the fault system becomes increasingly inefficient until a new forethrust grows. This fault growth reduces the W_{ext} by decreasing W_{fric} along the fault by an amount greater than the increase in W_{int} associated with the addition of the new fault. (C) If the forethrust were not to grow, the W_{ext} would continue to increase. The timing of fault growth depends on the work required to grow the new fault surface. The new fault grows at 10.5 cm thrust fault length rather than sooner in the experiment because the total energy reduction due to including the fault within the model (prefault W_{ext} – post fault W_{ext}) exceeds the energy consumed in the growth of the fault (W_{prop} and W_{seis}). Taken from DelCastello and Cooke, 2007.

Figure 7. Two models based on laboratory experiments on faults within gypsum slabs by Bobet and Einstein (1998). (A) Set-up for the numerical experiment of a 12.7 mm joint in a 160 x 80 mm slab of gypsum. The block is subject to $27.1e^{-6}$ m of uniaxial extension (u_v). E is Young's modulus and ν is Poisson's ratio. (B) Set-up for the numerical experiment on a 12.7 mm fault within gypsum that dips 60° from the vertical compressive stress, σ_v = -29 MPa. A confining pressure of σ_h = -2.5 MPa also is applied. Box shows location of (C). Box at fault tip is the location of the inset, showing pupative elements radial to the fault tip.

Figure 8. ΔW_{ext} per pupative element area from before growth to after growth of (A) the joint and (B) the fault models. Red markers are pupative element orientations where neither the tensile nor the shear failure criterion is met, so no growth can occur and there is no change in work. Green markers are orientations where the tensile strength is exceeded and failure can occur by opening. Blue markers are orientations where shear failure can occur. Tensile strength, T, is 3.2 MPa. Shear strength, S_o, is 78.7 MPa.

Figure 9. Work budgets for joint and fault propagation by one pupative element in the orientation that maximizes ΔW_{ext}. The energy to grow faults (W_{prop} + W_{seis}) comes from

ΔW_{int}. Growth elements for Fault 1 are not slip-weakening and do not experience a drop in strength during sliding. The inherent friction, μ_o = 0.3, is equal to the dynamic friction, μ_d. Growth elements for Fault 2 are slip-weakening, with μ_o = 0.6, μ_d = 0.3, and L = 4x10^{-6} m. Growth elements for Fault 3 also are slip weakening, with μ_o = 0.6, μ_d = 0.3, and L = 1x10^{-6} m. The most efficient propagation path for both the modeled joint and for all three faults is collinear at 180°.

Figure 10. (A) Planes carrying maximum tensile stress are perpendicular to the maximum tensile stress, σ_1 (top, green), while the two planes carrying the maximum Coulomb shear stress are oriented at angle φ to the maximum compressive strength, σ_3 (bottom, red). (B) Contours of the maximum tensile stress. (C) Contours of the maximum Coulomb shear stress, σ_c, on optimally oriented planes with μ_o = 0.3. (D) Tensile and Coulomb failure planes at 5 points located at one half the element length from the fault tip (0.0635 mm). Tensile strength, T, is 3.2 MPa. Shear strength, S_o, is 78.7 MPa. Strength must be exceeded for failure to occur (solid lines). Tensile and shear failure can occur at a variety of points around the fault tip, but this approach does not permit prediction of the favored propagation path for the fault.

Figure 1

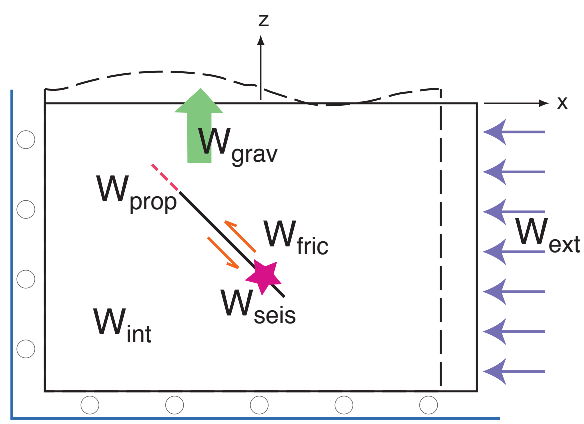

Figure 2

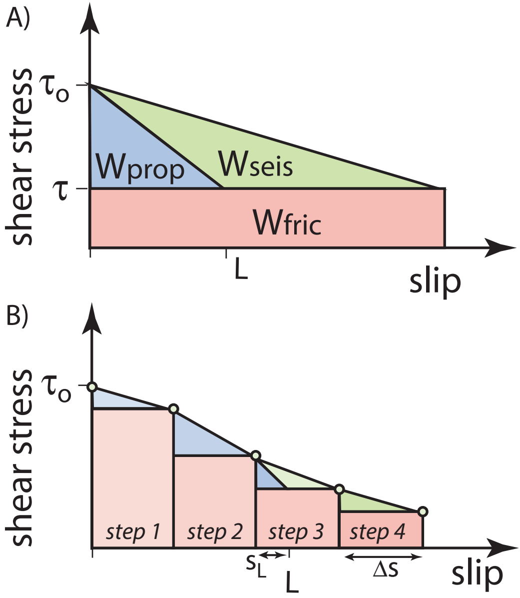

A)
shear stress
τo
τ
Wprop
Wseis
Wfric
L
slip
B)
shear stress
τo
step 1
step 2
step 3
step 4
sL
L
Δs
slip

Figure3

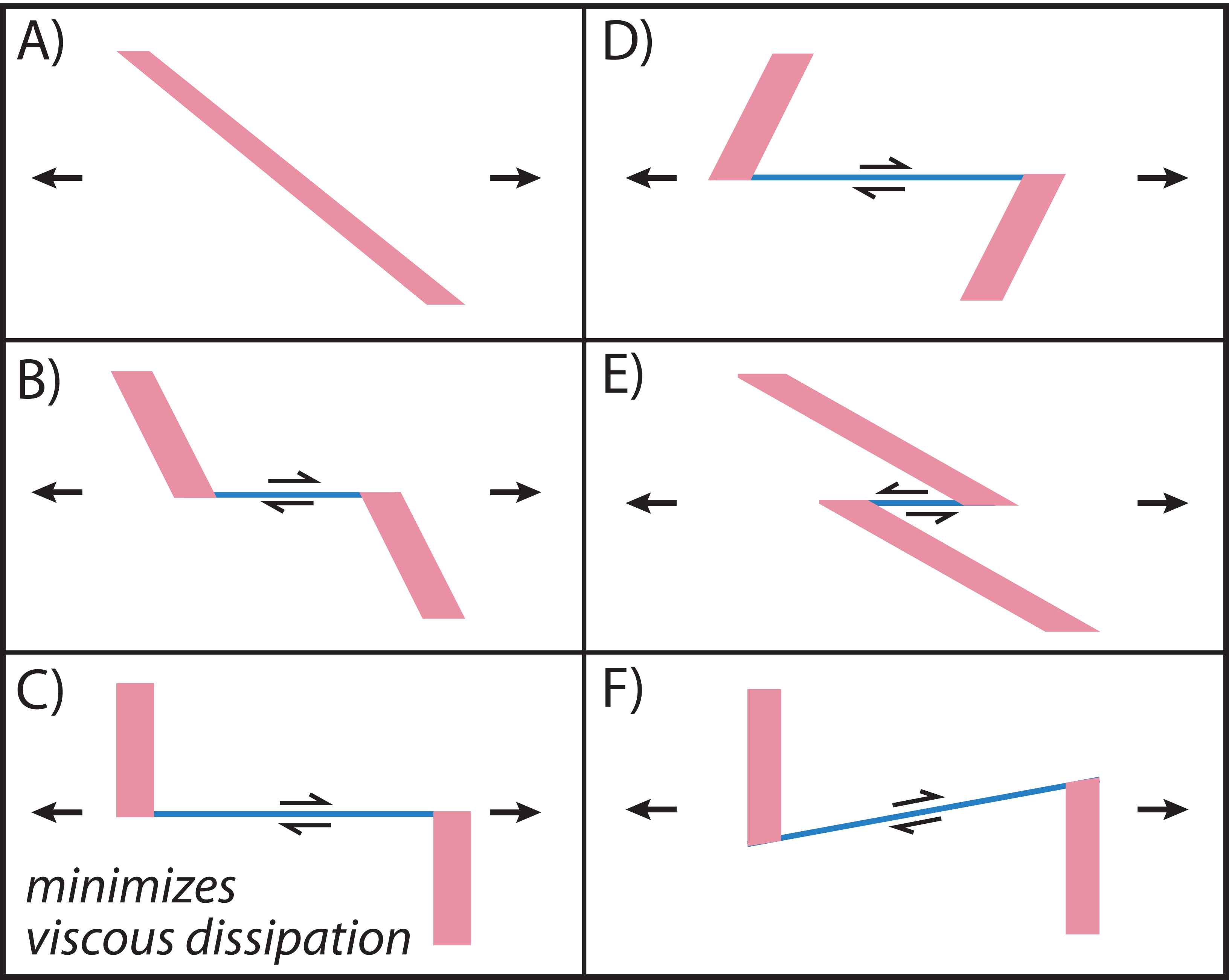

Figure4

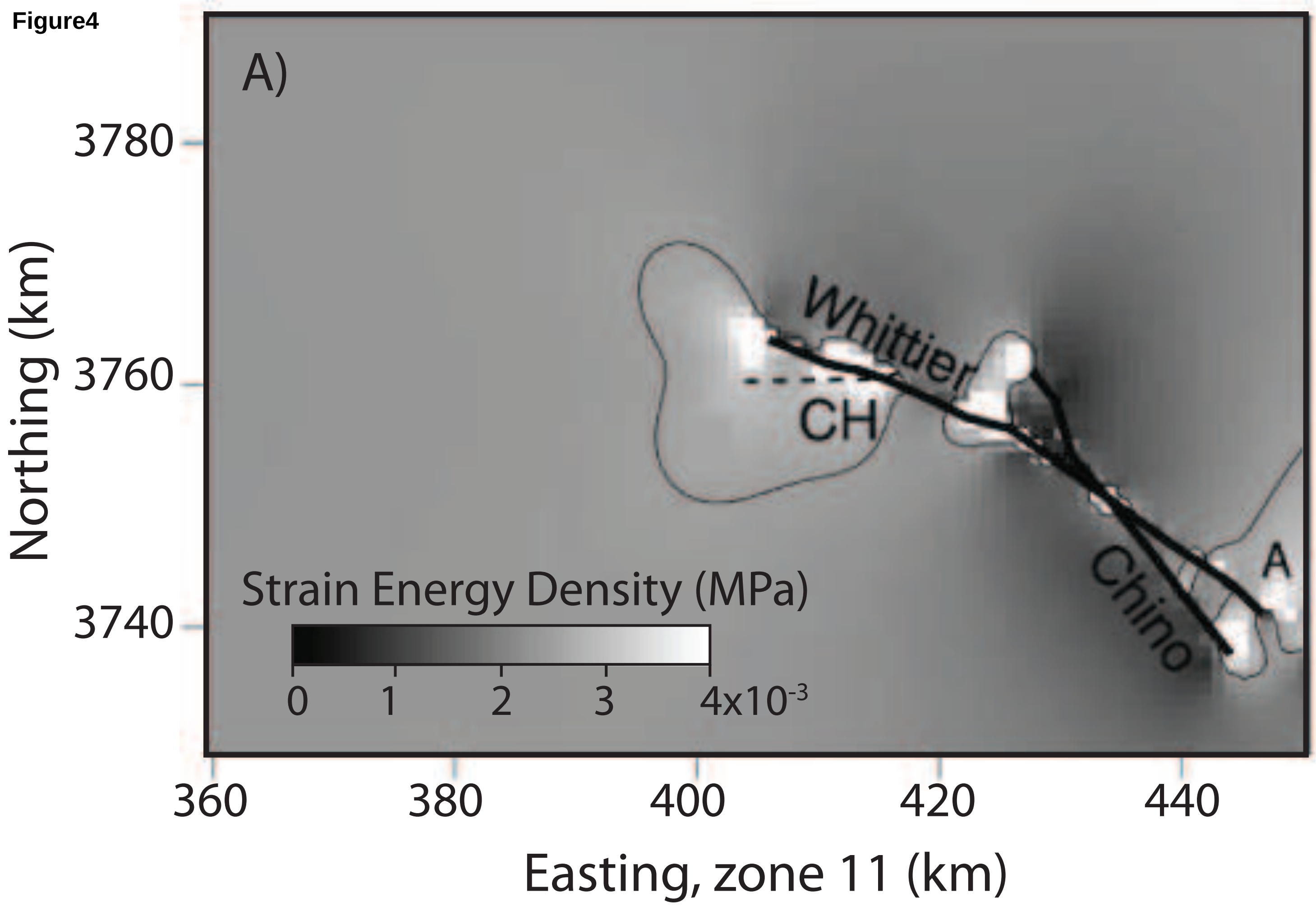
A)
3780
3760
3740
Northing (km)
Whittier
CH
Chino
A
Strain Energy Density (MPa)
0
1
2
3
4x10-3
360
380
400
420
440
Easting, zone 11 (km)

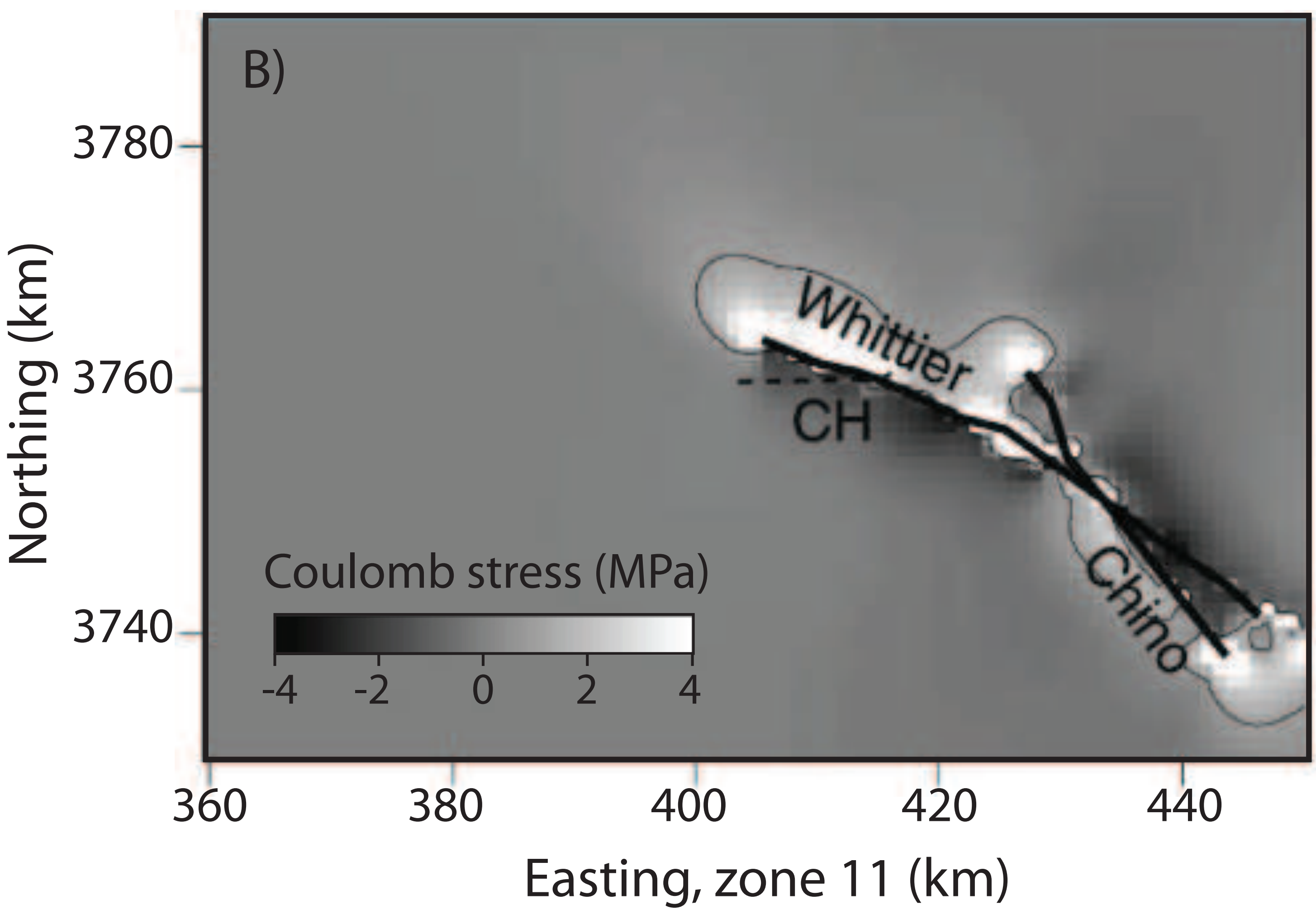
B)
3780
3760
3740
Northing (km)
Whittier
CH
Chino
Coulomb stress (MPa)
-4
-2
0
2
4
360
380
400
420
440
Easting, zone 11 (km)

Figure5

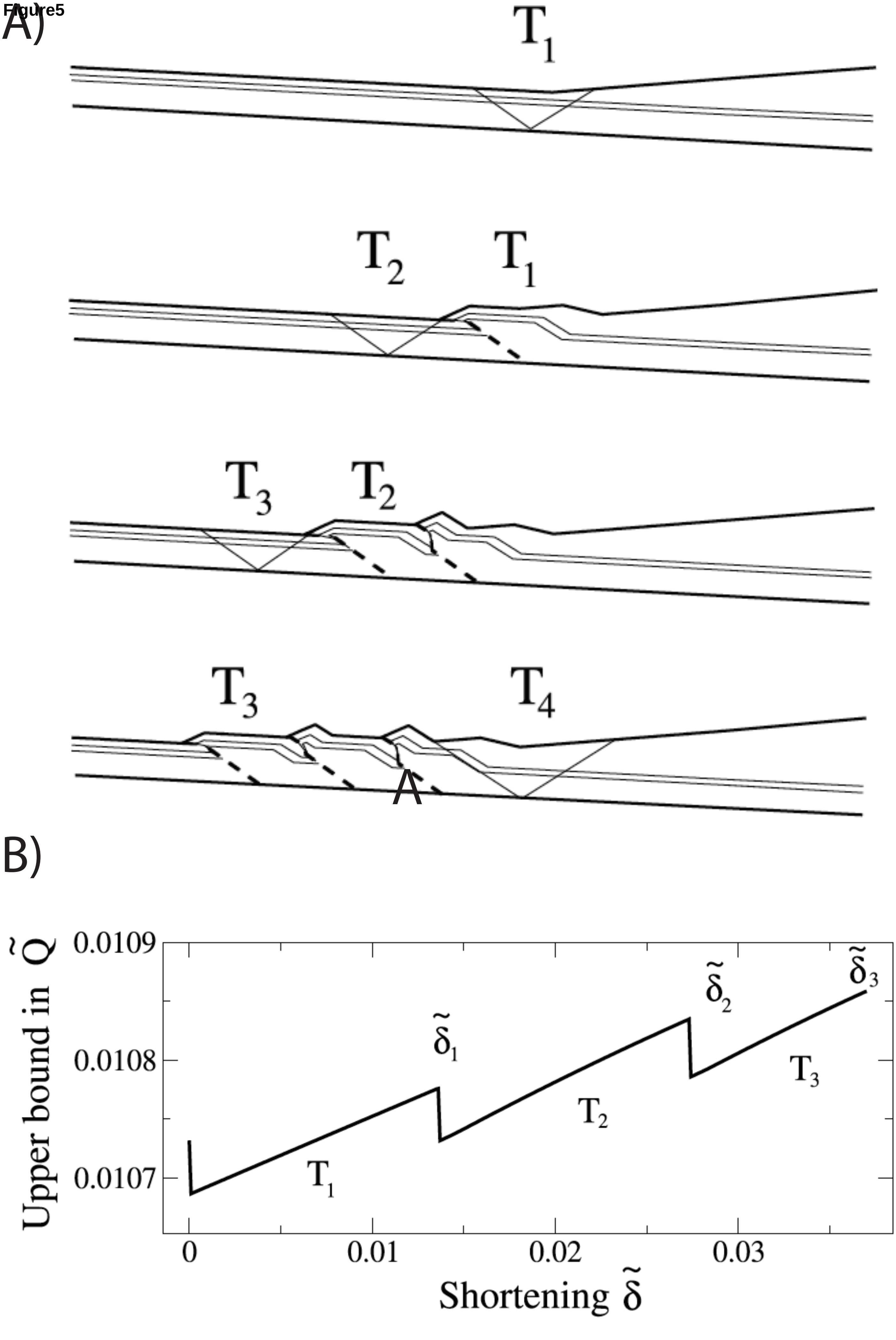

A)
T1
T2
T1
T3
T2
T3
T4
A
B)
Upper bound in Q̃
0.0109
0.0108
0.0107
δ̃1
δ̃2
δ̃3
T1
T2
T3
0
0.01
0.02
0.03
Shortening δ̃

Figure6

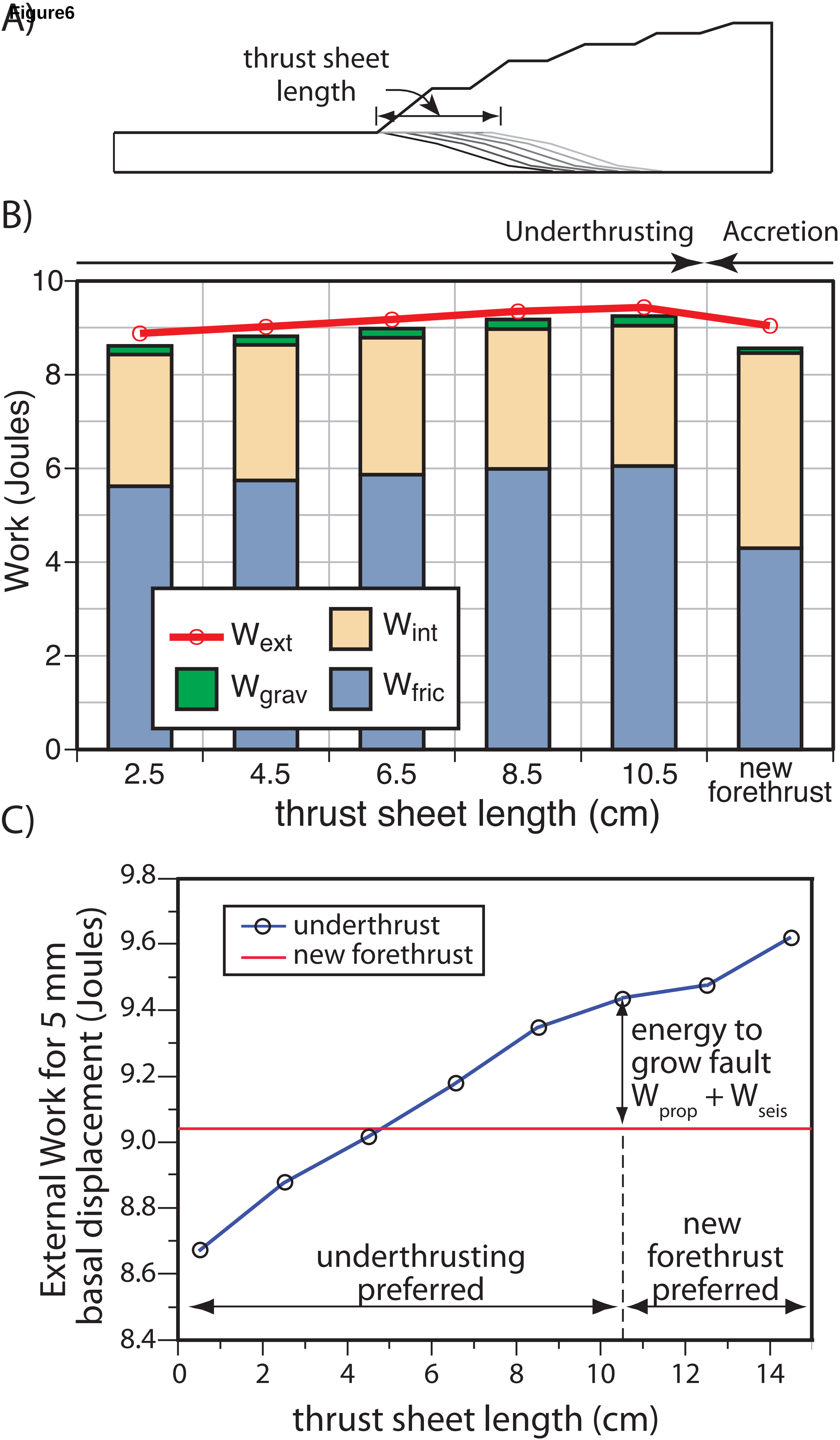
A)
thrust sheet
length
B)
Underthrusting
Accretion
Work (Joules)
10
8
6
4
2
0
Wext
Wint
Wgrav
Wfric
2.5
4.5
6.5
8.5
10.5
new
forethrust
thrust sheet length (cm)
C)
External Work for 5 mm
basal displacement (Joules)
9.8
9.6
9.4
9.2
9.0
8.8
8.6
8.4
underthrust
new forethrust
energy to
grow fault
Wprop + Wseis
underthrusting
preferred
new
forethrust
preferred
0
2
4
6
8
10
12
14
thrust sheet length (cm)

Figure 7

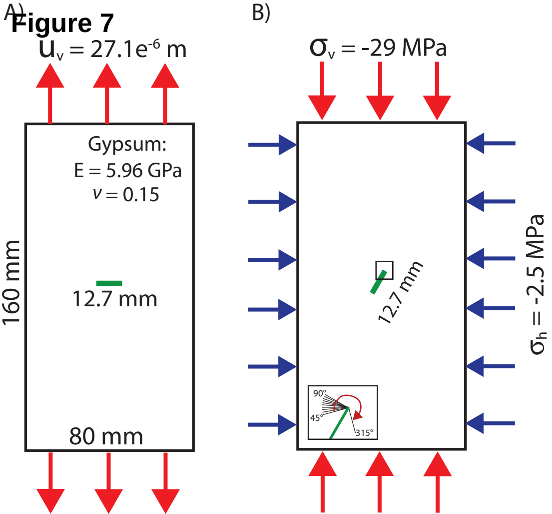

A)
$u_v = 27.1e^{-6}$ m
Gypsum:
E = 5.96 GPa
$\nu = 0.15$
160 mm
12.7 mm
80 mm
B)
$\sigma_v = -29$ MPa
12.7 mm
$\sigma_h = -2.5$ MPa
90°
45°
315°

Figure8

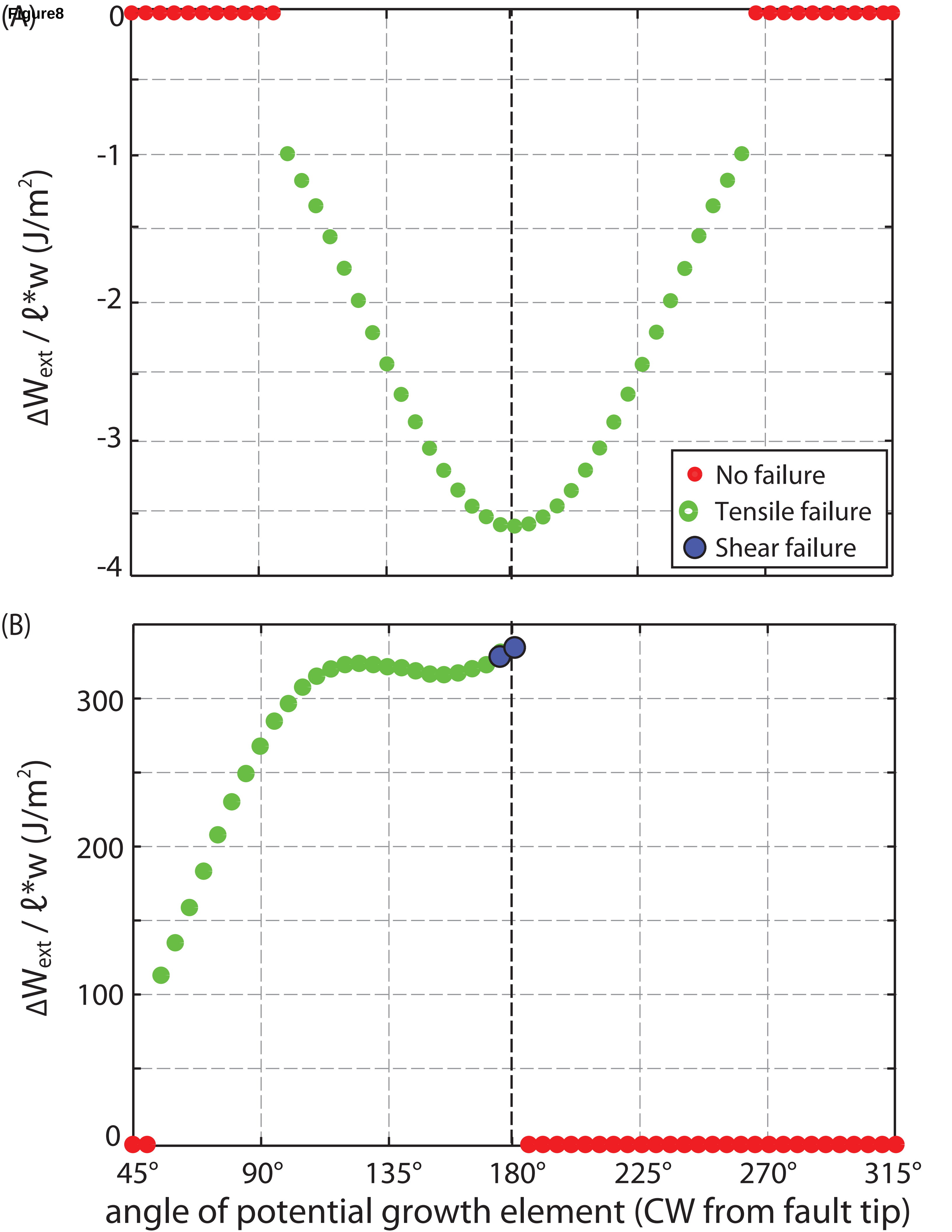

(A)
0
-1
-2
-3
-4
ΔW_ext / ℓ*w (J/m^2)
No failure
Tensile failure
Shear failure
(B)
300
200
100
0
ΔW_ext / ℓ*w (J/m^2)
45°
90°
135°
180°
225°
270°
315°
angle of potential growth element (CW from fault tip)

Figure 9

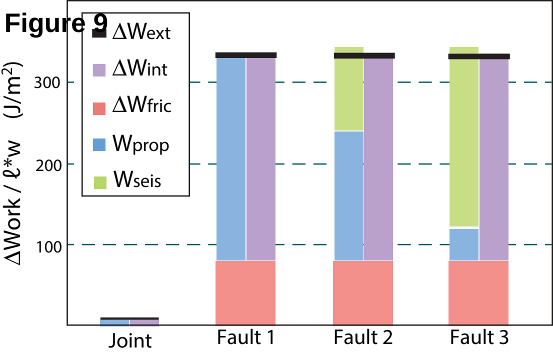
ΔWext
ΔWint
ΔWfric
Wprop
Wseis
ΔWork / ℓ*w (J/m²)
300
200
100
Joint
Fault 1
Fault 2
Fault 3

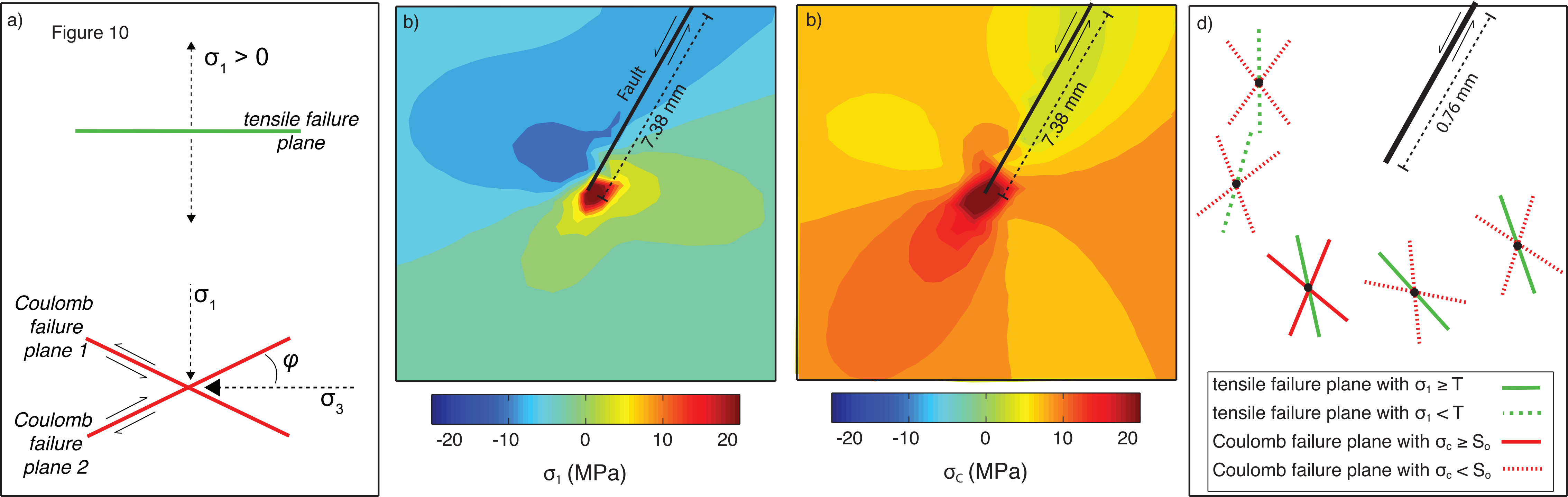

a)
Figure 10
σ1 > 0
tensile failure plane
σ1
Coulomb failure plane 1
Coulomb failure plane 2
φ
σ3
b)
Fault
7.38 mm
-20 -10 0 10 20
σ1 (MPa)
b)
7.38 mm
-20 -10 0 10 20
σC (MPa)
d)
0.76 mm
tensile failure plane with σ1 ≥ T
tensile failure plane with σ1 < T
Coulomb failure plane with σc ≥ So
Coulomb failure plane with σc < So

Table 1: Properties and work budgets for growing joint and fault models

Scenario	μ_s	μ_d	L (m)	W_{prop} (J/m^2)	W_{seis} (J/m^2)	ΔW_{fric} (J/m^2)	$W_{prop} + W_{seis} + \Delta W_{fric}$ (J/m^2)	ΔW_{int} (J/m^2)	ΔW_{ext} (J/m^2)
Joint	0	0	0	3.62	0.00	0.00	3.62	3.63	3.63
Fault 1	0.3	0.3	0	260.77	0.00	79.78	340.54	254.05	333.83
Fault 2	0.6	0.3	$1e^{-6}$	158.60	102.14	79.45	340.19	254.38	333.83
Fault 3	0.6	0.3	$4e^{-6}$	39.70	221.11	79.45	340.26	254.38	333.83